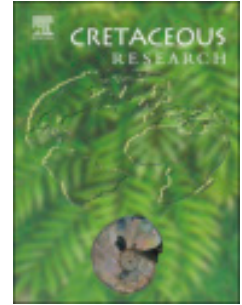


Journal Pre-proof

TAPHONOMY AND PALEOHISTOLOGY OF A DINOSAUR RIB FROM MARÍLIA FORMATION, BAURU GROUP, IN THE STATE OF MINAS GERAIS, BRAZIL

Vinícius José Maróstica Paio, Isabela Jurigan, Rafael Delcourt, Rafael Souza de Faria, Alessandro Batezelli, Fresia Ricardi-Branco



PII: S0195-6671(24)00072-7

DOI: <https://doi.org/10.1016/j.cretres.2024.105899>

Reference: YCRES 105899

To appear in: *Cretaceous Research*

Received Date: 2 June 2023

Revised Date: 30 March 2024

Accepted Date: 30 March 2024

Please cite this article as: Paio, V.J.M., Jurigan, I., Delcourt, R., de Faria, R.S., Batezelli, A., Ricardi-Branco, F., TAPHONOMY AND PALEOHISTOLOGY OF A DINOSAUR RIB FROM MARÍLIA FORMATION, BAURU GROUP, IN THE STATE OF MINAS GERAIS, BRAZIL, *Cretaceous Research*, <https://doi.org/10.1016/j.cretres.2024.105899>.

This is a PDF file of an article that has undergone enhancements after acceptance, such as the addition of a cover page and metadata, and formatting for readability, but it is not yet the definitive version of record. This version will undergo additional copyediting, typesetting and review before it is published in its final form, but we are providing this version to give early visibility of the article. Please note that, during the production process, errors may be discovered which could affect the content, and all legal disclaimers that apply to the journal pertain.

© 2024 Elsevier Ltd. All rights reserved.

1 **TAPHONOMY AND PALEOHISTOLOGY OF A DINOSAUR RIB**
2 **FROM MARÍLIA FORMATION, BAURU GROUP, IN THE STATE**
3 **OF MINAS GERAIS, BRAZIL**

4
5 Vinícius José Maróstica Paio^{a*}, Isabela Jurigan^a, Rafael Delcourt^{b,d}, Rafael
6 Souza de Faria^c, Alessandro Batezelli^a, Fresia Ricardi-Branco^a

7
8 ^a *Universidade Estadual de Campinas (UNICAMP), Instituto de Geociências, Departamento de*
9 *Geologia e Recursos Naturais, Rua Carlos Gomes, 250, 13083-855, Cidade Universitária,*
10 *Campinas, São Paulo, Brazil.*

11
12 ^b *Universidade de São Paulo, Departamento de Biologia, Faculdade de Filosofia, Ciências e*
13 *Letras de Ribeirão Preto, Laboratório de Paleontologia, Av. Bandeirantes, 3900, 14040-901,*
14 *Monte Alegre, Ribeirão Preto, São Paulo, Brazil.*

15
16 ^c *Pontifícia Universidade Católica de Campinas (PUC-Campinas), Centro de Ciências da Vida,*
17 *Faculdade de Ciências Biológicas, Av. John Boyd Dunlop, s/n, 13060-904, Jd. Ipaussurama,*
18 *Campinas, São Paulo, Brazil.*

19
20 ^d *Bayerische Staatssammlung für Paläontologie und Geologie, Richard-Wagner-Straße 10,*
21 *80333 München, Deutschland*

22
23 ^{*} *Corresponding author. Universidade Estadual de Campinas (UNICAMP), Instituto de*
24 *Geociências, Departamento de Geologia e Recursos Naturais, Rua Carlos Gomes, 250, 13083-*
25 *855, Cidade Universitária, Campinas, SP, Brazil.*

26

27 *E-mail addresses:* dinicio.jmp@gmail.com (V.J.M. Paio), isajurigan@gmail.com (I. Jurigan),
28 rafael.delcourt@gmail.com (R. Delcourt), rafael.faria@puc-campinas.edu.br (R.S. Faria),
29 batezeli@unicamp.br (A. Batezelli), fresia@unicamp.br (F. Ricardi-Branco).

30

Journal Pre-proof

31

ABSTRACT

32 The Bauru Group (Campanian–Maastrichtian) has one of the richest fossil
33 records of Cretaceous in South America. All dinosaur fossils from this unit were
34 assigned to Saurischia, most of them poorly preserved. We present the
35 histological and taphonomic analysis of a dinosaur dorsal rib fragment from the
36 Marília Formation in the western state of Minas Gerais. Thin sections were
37 prepared to describe the microstructures of the bone tissue and the fossilization
38 processes involved in preserving the specimen. An elemental analysis was also
39 performed to verify the chemical composition of the fossil and rock matrix.
40 Haversian bone was identified in the rib cortex, and no growth marks or an
41 external fundamental system were found. The rib probably belonged to a
42 saurischian dinosaur because of its plank shape and elliptical cross-section.
43 Hypotheses regarding taphonomic processes were inferred. An extended period
44 of subaerial exposure, followed by high-energy transport, was interpreted due to
45 extensive fractures and signs of abrasion on the outer surface of the bone. Pyrite
46 pseudomorphs (framboids) indicate that the bone was deposited in a reductive
47 environment. After burial, the rapid precipitation of calcite and alkaline stability
48 allowed the preservation of apatite during the recrystallization phase. The
49 manganese hydroxides were deposited on apatite crystals during early
50 diagenesis. We concluded that the fossil rib presented a common taphonomic
51 bias identified among vertebrate fossils of the Bauru Group, which is associated
52 with the exposure of the bones to arid and semiarid climates, their transport into
53 the depositional environments and pedogenetic influence during fossil
54 diagenesis.

55

56 Keywords: Osteohistology. Bone Weathering. Fossil diagenesis. Bauru Basin.

57

Journal Pre-proof

58

59 **1. INTRODUCTION**

60 The Bauru Group is one of the richest sites for paleo-vertebrates from the
61 Cretaceous of South America (Brusatte et al., 2017; Candeiro et al., 2020; Geroto
62 and Bertini, 2014; Langer et al., 2022; Martinelli and Teixeira, 2015). Its dinosaur
63 fossil records are restricted to saurischians, represented by theropods and
64 sauropods, the last of which is exclusively composed of titanosaurs, with 11
65 recognized species (Faria et al., 2015; Navarro et al., 2022; Silva Junior et al.,
66 2022). For theropods, only three species have been described: the abelisaurids
67 *Thanos simonattoi* Delcourt and Iori, 2020 and *Kurupi itaata* Iori et al., 2021, and
68 the unenlagiine maniraptoran *Ypupiara lopai* Brum et al., 2021b. However, most
69 of the dinosaur fossils in the Bauru Group are isolated or disarticulated bone
70 fragments (Candeiro et al., 2019; Cavalcanti et al., 2021; Delcourt and Langer,
71 2022; Silva Junior et al., 2017) and numerous theropod teeth (Candeiro et al.,
72 2017; Delcourt et al., 2020; Tavares et al., 2014). Despite the poor preservation
73 of diagnostic characteristics, fossils contain relevant paleoecological information,
74 such as signs of predation (Reis et al., 2023), saprophagous organism activities
75 (Paes Neto et al., 2018), and illnesses and parasite-host relationships (Aureliano
76 et al., 2021b).

77 Paleohistological studies have contributed to a considerable number of
78 recent discoveries involving the ontogeny, phylogeny, biomechanics, and
79 paleoenvironment of dinosaurs and other extinct organisms (Bailleul et al., 2019;
80 Chinsamy, 2023; Padian, 2013). Based on petrography and histology,
81 paleohistological techniques include preparing, cutting, and mounting fossils on
82 thin sections to analyze microscopic structures preserved inside bones, tendons,

83 eggshells, or other tissues (Lamm, 2007). Paleohistological analyses have been
84 applied to study Brazilian dinosaur records covering several fields of research;
85 for instance, ontogenetic identification (Ghilardi et al., 2016; Sayão et al., 2020;
86 Souza et al., 2020), description of osteohistological structures, and
87 paleopathology (Aureliano et al., 2021b, 2021a; Barbosa et al., 2016; Brum et al.,
88 2021a).

89 Paleohistological techniques can provide insight into the taphonomy of a
90 fossil. Bone structure and tissues can preserve evidence of pre-burial processes
91 such as decomposing organisms (Kremer et al., 2012; Owocki et al., 2016) and
92 bone exposure (Pfretzschner and Tütken, 2011; Previtiera, 2019, 2017).
93 Additionally, minerals deposited within the internal spaces of bones can indicate
94 sub-surface conditions that favored fossil diagenesis and its changes over time
95 (Clarke, 2004). Authigenic minerals provide information about the depositional
96 paleoenvironment, such as oxidation levels and pH, when analyzed for their
97 composition (Wings, 2004). They are also useful for comparing diagenetic
98 processes in different formations (Rogers et al., 2020).

99 However, taphonomic studies of vertebrate fossils from the Bauru Group
100 (Upper Cretaceous) are rare and have only been applied to a few tetrapod groups
101 such as crocodylomorphs (Araújo Júnior and Marinho, 2013; Vasconcellos and
102 Carvalho, 2006) and testudines (Bertini et al., 2006). Studies comparing the
103 modes of preservation of different taxa are even rarer (Azevedo et al., 2013;
104 Bandeira et al., 2018). Regarding fossil diagenetic patterns, Garcia et al. (2005)
105 proposed a general model for bone microstructure preservation in the Uberaba,
106 Adamantina, and Marília formations. In recent years, only three studies on the
107 fossil diagenesis of bones in the Bauru Group have been published. The research

108 of Marchetti et al. (2019) examined specimens of the crocodylomorph
109 *Montealtosuchus arrudacamposi* Carvalho et al., 2007, from the Adamantina
110 Formation. Pinto et al. (2020) conducted a geochemical analysis of turtle bone
111 fragments collected from the outcrops of the Presidente Prudente Formation,
112 which is equivalent to part of the Adamantina Formation (Fernandes and
113 Coimbra, 2000), in Pirapozinho, São Paulo, Brazil. Both studies concluded that
114 bone preservation was facilitated by the recrystallization of apatite during early
115 diagenesis, a process that may have been promoted by groundwater saturated
116 with carbonates and fluorine (Marchetti et al., 2019; Pinto et al., 2020). In a
117 histological study of titanosaur vertebrae from the Marília Formation, Aureliano et
118 al. (2020) suggested that diagenetic scenarios played an essential role in
119 preserving bone tissue (pneumosteum).

120 This study aimed to improve our understanding of the paleoenvironment
121 of the Bauru Group (Upper Cretaceous) and the fossil diagenesis of its dinosaur
122 bones through the histotaphonomic characterization of the fossil rib fragment
123 CP2/200A-B from the Marília Formation. The specimen was found in the western
124 part of Minas Gerais, known as the Triângulo Mineiro region, and was interpreted
125 as belonging to an indeterminate saurischian dinosaur.

126

127 1.1. Geological Context

128 The Bauru Basin consists of an intracratonic depression that sustained
129 the deposition of an inland continental sedimentary sequence after separating the
130 South American Plate from the Gondwana continent (Fernandes and Coimbra,
131 2000; Menegazzo et al., 2016). This basin covers an area of approximately
132 379,000 km², is located almost exclusively in Brazil, and occupies the western

133 region of São Paulo and Minas Gerais states, Southern Goiás, Eastern Mato
134 Grosso do Sul, and the Northwest of Paraná state (Fernandes and Coimbra,
135 2000; Menegazzo et al., 2016). The Bauru Basin is Aptian–Maastrichtian and is
136 composed of sandstones and sandy mudstone deposits at the bottom and
137 sandstones and conglomerates at the top (Batezelli, 2017). The Bauru Basin is
138 subdivided into Caiuá and Bauru groups (Fernandes and Coimbra, 2000). The
139 Bauru Group (Campanian–Maastrichtian) is represented by the Araçatuba,
140 Adamantina, Uberaba, and Marília formations (Batezelli, 2017; Batezelli and
141 Ladeira, 2016; Castro et al., 2018), as well as the Serra da Galga Formation,
142 proposed based on recent studies carried out on the former Serra da Galga
143 Member of the Marília Formation (Soares et al., 2021).

144 The fossil fragment (CP2/200A-B) was collected from an outcrop of the
145 Marília Formation located at kilometer 159 of the BR 364 highway (Figure 1)
146 between Campina Verde and Gurinhatã, in Minas Gerais, Brazil. The
147 stratigraphic unit is characterized by sandstones, conglomerates, and paleosols
148 cemented by calcium carbonate and silica, which comprise the fluvial facies
149 (Batezelli, 2017). Batezelli et al. (2019) analyzed outcrops of the Bauru Group in
150 the Triângulo Mineiro region and identified them as part of the facies association
151 called Campina Verde paleosol sequence (Figure 1). According to the authors,
152 the deposits that were formed in an environment composed of ephemeral rivers,
153 eolian dunes, and paleosols correspond to the medial portion of the distributive
154 and progradational fluvial system of the northeastern region of the Bauru Group.
155 The prospective stratum of the fossil is characterized as a Ck (Figure 1) horizon
156 paleosol (inceptisol/entisol) developed under the influence of a semiarid climate
157 Batezelli et al. (2019).

158

159

160 2. MATERIALS AND METHODS

161 The fossil rib fragment is housed in the Scientific Collection of Vertebrate
162 Paleontology (CP2) at the Instituto de Geociências (IG), Universidade Estadual
163 de Campinas (UNICAMP), under the collection number CP2/200A-B. The
164 specimen measured approximately 50 mm in proximodistal length, 60 mm in
165 anteroposterior width, and 27 mm in mediolateral height in cross-section prior to
166 sectioning (Figure 2). Partial erosion exposed a portion of the medullary
167 spongiosa on one of the dorsal rib surfaces (Figure 2).

168

169 2.1. Petrographic and Elemental Analyses

170 The rib fragment was cross-sectioned, and two petrographic thin sections
171 were produced according to standard paleohistological techniques (Chinsamy
172 and Raath, 1992; Lamm, 2013). For a more detailed analysis of the rock matrix,
173 the petrographic slides were polished to a thickness of 30 μm (Marchetti, 2017).

174 The samples were analyzed at the Laboratory of Paleohydrogeology at
175 UNICAMP using a Carl Zeiss Scope A1 ZEISS petrographic microscope under
176 normal and cross-polarized light using a gypsum compensator. A ZEISS
177 AxioCam camera captured images, and the microscope software Zenlite from
178 ZEISS Microscopy was used to visualize and treat the images. The thin section
179 received carbon coverage, and elemental analysis was performed using an LEO
180 430i model Scanning Electron Microscope (SEM) equipped with an energy
181 dispersive detector (EDS) manufactured by Oxford Instruments. The SEM was

182 operated at 67 eV in vacuum mode at the Laboratory of Mineral Quantification at
183 the Instituto de Geociências at UNICAMP.

184

185 **2.2. Paleohistological Analysis**

186 Histological descriptions of the sections were performed according to the
187 standard nomenclature of microstructures and classifications of bone tissues, as
188 grouped by de Buffrénil and Quilhac (2021). Considering the fossil bone to be a
189 fragment of a dorsal rib, our interpretation of the ontogenetic stage of the
190 specimen was based on current models and hypotheses regarding the growth
191 and development of this type of bone in sauropod dinosaurs (Brum et al., 2022;
192 Gallina, 2012; Waskow and Sander, 2014). In addition, three histological
193 parameters for ontogenetic analysis developed by Mitchell and Sander (2014)
194 were used: (i) the apposition front (AF), which represents the deposition of
195 primary bone tissue on the periosteal surface; (ii) the Haversian substitution front
196 (HSF), which indicates the deposition of secondary osteons; and (iii) the
197 resorption front (RF), which characterizes the resorption of bone tissue and
198 expansion of the medullary cavity.

199

200

201 **3. RESULTS**

202

203 **3.1. Taxonomy**

204 Based on its flattened shape, the fossil was first compared with published
205 data on other rib specimens found in the Marília Formation and correlated
206 geological units of the Bauru Group (e.g. Baiano and Cerda, 2023; Bertini et al.,

207 2001; Coria et al., 2013; O'Connor, 2007; Santucci and Arruda-Campos, 2011;
208 Silva Junior et al., 2022; Silva Junior et al., 2019). For example, the sauropod rib
209 specimens reported by Bertini et al. (2001) were similar in size to those studied
210 in the present study. In the appendix of the publication, the authors describe up
211 to 44 rib fragments assigned to Titanosauria that were found in an outcrop of the
212 Marília Formation (Echaporã Member) in Monte Alto, São Paulo. The specimens
213 are stored in the collection of the Museu de Paleontologia 'Professor Antônio
214 Celso de Arruda-Campos' (MPMA) located in Monte Alto. Among these fossils,
215 four ribs (MPMA-04) were 932 mm long and 55.5 mm average wide. Six other rib
216 fragments (MPMA-06) listed in this article were 48 and 80 mm wide. By
217 comparing the measurements with the CP2/200A-B specimen, the width
218 corresponded to the average size observed in previous studies.

219 The fossil morphology presented in this study places it in a more inclusive
220 group. Wilson (2002) proposed the anterior dorsal ribs with a plank-like shape,
221 whose anteroposterior width was three times larger than their mediolateral length,
222 as a synapomorphy of Titanosauriformes. Fossil rib CP2/200A-B had
223 approximate measurements of 60 and 27 mm for these parameters. The
224 morphology of the fragment is like that described for the dorsal rib shafts of
225 *Overosaurus paradasorum* (Coria et al., 2013) of the Anacleto Formation
226 (Campanian) in Argentina (Garrido, 2010). *O. paradasorum* has an elliptical or
227 lateromedially flattened shape, in cross-section, of the distal shaft of both the third
228 and fourth pairs of anterior ribs, and the posterior dorsal ribs. The maximum
229 anteroposterior width determined for *O. paradasorum* dorsal ribs is also like
230 CP2/200A-B with sizes ranging from 70 mm (third rib pair), 65 mm (first right rib),
231 and 55 mm (fourth rib pair) (Coria et al., 2013).

232 Compatibility with a large South American theropod dinosaur was
233 determined by comparing the ribs identified and described in the literature.
234 Abelisaur dorsal ribs commonly have an anterior intercostal ridge (Filippi et al.,
235 2018; Méndez et al., 2022; O'Connor, 2007), but this structure was absent in the
236 CP2/200A-B fossil. The distal shafts of the second and third dorsal ribs of
237 *Majungasaurus crenatissimus* (Depéret, 1896) (see O'Connor, 2007) and the
238 distal sections of the dorsal ribs of *Aucasaurus garridoi* Coria et al., 2002 (see
239 Baiano and Cerda, 2023) exhibited a mediolaterally flattened shape in the cross-
240 section, which is like the titanosaur specimens mentioned earlier here. These
241 features are conflicting and insufficient to assign the bone fragment CP2/200A-B
242 to abelisaur or titanosaurs with conviction. Megaraptors, another group of
243 carnivorous dinosaurs, have posterior and anterior intercostal ridges, as well as
244 intercostal grooves on their dorsal rib shafts (Aranciaga Rolando et al., 2022;
245 Lamanna et al., 2020; Porfiri et al., 2014). Neither of these features was identified
246 in the fossil CP2/200A-B. Therefore, the hypothesis that the specimen belonged
247 to a megaraptorid theropod was rejected.

248

249 3.2. Histological analysis

250 Regarding the composition of bone tissues in both thin sections, we
251 identified a 6-mm-thick dense Haversian bone throughout the length of the rib
252 cortex (Figures 3 and 4). Secondary osteons presented overlaps, indicating one
253 or more generations of bone remodeling (Figures 3C and 4B). A large area of
254 cancellous bone up to 10 mm thick was observed in the medullary region, with
255 trabeculae and erosion cavities derived from bone reabsorption (Figures 3E and

256 4C). The same secondary osteonal structures were observed in the cortex on
257 both sides of the rib. Lines of arrested growth (LAGs) are absent.

258 On the outer surface of the cortex in the periosteal region, the osteons
259 were severely damaged, part of them with half of their structures eroded (Figures
260 3C and 4B). No external fundamental system (EFS) or associated lamellar tissue
261 is preserved in this region of the compact bone. The endosteal region was poorly
262 preserved, and several parts of the lamellar tissue were replaced by calcite. We
263 also identified deep and wide fractures extending into the medullary cavity of the
264 rib (Figure 3B and 3E), sometimes filled with a rock matrix or calcitic cement,
265 forming veins. However, the mineralogical composition of the bone tissue was
266 preserved, with a predominance of apatite $[\text{Ca}_5(\text{PO}_4)_3]$ in all areas, as predicted
267 in the EDS analysis (see Supplementary Material).

268 Some considerations were made regarding the possible stages of
269 ontogenetic development of the specimen. According to recent proposals for the
270 development of bone tissue in sauropod ribs, advanced HSF and RF limited to
271 the perimedullary region suggest an adult or senescent individual (Brum et al.,
272 2022). However, no confident statement about the ontogeny can be made
273 because of the absence of an EFS and the unknown position of the fragment in
274 the length of the rib (see Discussion section). EFS represents the deceleration of
275 bone deposition (AF).

276

277 3.3. Petrographic analysis

278 A calcitic matrix and cement characterized thin sections of the rib
279 fragment (CP2/200A-B) in the medullary region and the outer surface of the bone
280 as veins (Figures 3C, 3E and 4C). The internal spaces are mainly filled with

281 spathic calcite ($\sim 0.35 \mu\text{m}$). On the surface of the rib trabeculae, a recrystallized
282 calcite phase was identified under polarized light, with a slight fringe at the edges
283 of the structures along their entire perimeters (Figures 3E and 5D). In addition,
284 we observed deposits of opaque minerals inside the Haversian canals and
285 osteocyte cavities. According to EDS analysis, the minerals correspond to iron
286 oxides, which have a framboidal habit (see Supplementary Material) and
287 constitute pyrite pseudomorphs. In addition, deposits of opaque minerals in a
288 dendritic pattern were observed, percolating out of the vascular canal and
289 covering the lamellae of secondary osteons (Figure 3D), consistent with
290 manganese oxides.

291 The sample was associated with calcitic cement sandstone, with poorly
292 selected grains ranging from coarse sand (0.70 mm) to very fine sand (0.10 mm),
293 although it was predominant in the fine sand fraction (0.19 mm). The larger grains
294 (medium and coarse sand fractions) exhibited variable roundness ranging from
295 sub-rounded to well-rounded. Smaller grains exhibited more angular shapes
296 ranging from angular to subangular. The mineral grains are predominantly
297 composed of quartz, plagioclase feldspar, and alkali feldspar (microcline and
298 orthoclase) (Figure 5C and 5D). Under cross-polarized light, grains of
299 monocrystalline quartz with straight and undulating extinction and polycrystalline
300 quartz were observed (Figure 5A). Most polycrystalline or undulating extinction
301 quartz grains occurred in the coarse and medium sand fractions, with little
302 contribution from straight extinction quartz. However, the monocrystalline grains
303 of straight extinction are limpid and concentrated mainly in finer particles. Overall,
304 the minerals exhibited fractures and slightly corroded edges associated with
305 calcite replacement (Figure 5B and 5D).

306 The two thin sections exhibited a few unique structures. On petrographic
307 slide 234 (CP2/200A), a few unidentified grains of a brownish color and peloidal
308 texture were found. However, on slide 235 (CP2/200B), a small number of grains
309 configured a residual texture filled with calcite laths, which may have been
310 associated with volcanic lithic fragments (Figure 5E and 5F).

311

312

313 **4. DISCUSSION**

314

315 **4.1. Taxonomy and ontogeny**

316 The similarities in size between fossil CP2/200A-B and other titanosaur
317 specimens described from the same geological unit (Bertini et al., 2001) along
318 with the plank-like morphology of the rib (Wilson, 2002) and its elliptical shape in
319 cross-section (Coria et al., 2013), suggest that the specimen may belong to the
320 Titanosauria group. However, there are exceptions to dorsal rib morphology in
321 some titanosaur species, including those found in the Bauru Group. For example,
322 the recognized specimens of *Uberabatitan ribeiroi* Salgado and Carvalho, 2008
323 (see Silva Junior et al., 2019), whose dorsal ribs present the medial part of the
324 shaft slightly concave, and the holotype of *Arrudatitan maximus* (Santucci and
325 Arruda-Campos, 2011) (Silva Junior et al., 2022), which has mid-thorax ribs with
326 well-developed anterior and posterior ridges in the proximal shaft, acquiring a “D”
327 shape in cross-section. Even the *Overosaurus* ribs used for comparison in this
328 study present laminar projections on the posterior face of the proximal shaft of
329 the second and third anterior dorsal ribs, which are considered diagnostic
330 characteristics of the species (Coria et al., 2013).

331 A mediolaterally flattened shape may be identified in the ribs of other
332 taxa, such as the distal shaft of the anterior dorsal ribs of the abelisaurid
333 *Majungasaurus* (O'Connor, 2007). Degradation of one of the fragment's faces
334 during telodiagenesis precludes the identification of an anterior intercostal ridge,
335 which is also present in abelisaurid theropods (Aranciaga Rolando et al., 2021;
336 Filippi et al., 2018; Méndez et al., 2022; O'Connor, 2007). Histological
337 comparison of the dorsal ribs was insufficient for decisive taxonomic classification
338 because of similarities in bone tissue and microstructure, such as the thickness
339 ratio of the medullary cavity and cortex, and advanced remodeling, which were
340 found in both the dorsal ribs of *Aucasaurus garridoi* (Baiano and Cerda, 2023)
341 and titanosaur species of the Bauru Group (Brum et al., 2022; Windholz et al.,
342 2023). Thus, owing to the high fragmentation of fossil CP2/200A-B and the
343 absence of clear diagnostic characters attributed to abelisaurids, as exemplified
344 above, we identified it as an indeterminate saurischian dinosaur from the Marilia
345 Formation.

346 To assess the ontogenetic stage of the organism, some characteristics
347 of the studied sample were unable to be identified precisely, such as the absence
348 of recognizable LAGs, growth rings, and EFS. The absence of the latter
349 histological structure may be related to extensively damaged secondary osteons
350 present on the surface of the cortex (Figures 3C and 4B), as discussed in the
351 next section. Based on the current interpretations of rib bone development (Brum
352 et al., 2022), we could only classify the organism as adult or senescent. However,
353 the sampling location of the bone may have influenced the interpretation of the
354 results. According to Waskow and Sander (2014), the posteromedial side of the
355 proximal end of the rib shaft is the area with optimal growth record. The

356 proximodistal growth direction of bone justifies this characteristic during
357 ontogeny, with resorption and secondary deposition induced by mechanical
358 stress. It promotes intra-elemental histovariability with significant bone
359 remodeling in more distal regions, reducing the number of recognizable growth
360 rings at these sites (Gallina, 2012; Waskow and Sander, 2014). Since it is a
361 fragment and its position in the rib length is possibly distal, remodeling may not
362 represent an adult organism but a tissue adaptation to mechanical pressure
363 applied at the distal and lateral ends of the bone.

364

365 **4.2. Taphonomy**

366 Based on the petrographic and histological characteristics of sample
367 CP2/200A-B, we inferred the taphonomic processes recorded during its
368 preservation. The presence of damage to the secondary osteons on the outer
369 surface of the rib suggests that the bone was worn away during transport (Figures
370 3C and 4B). This feature is attested by the calcitic cement in the rib medullary
371 cavity, veins, and rock matrix as well as the presence of grains inside the larger
372 cracks (Figure 3B and 3E). The occurrence of these fractures may be associated
373 with the weathering of bones exposed to the ground surface under semiarid
374 conditions (Behrensmeyer, 1978). Subaerial exposure for months or years before
375 burial is a typical taphonomic pattern in vertebrate fossils of the Bauru Group
376 because a considerable amount of material has been fragmented or isolated
377 (Azevedo et al., 2013; Bandeira et al., 2018, 2016; Brum et al., 2021b; Delcourt
378 and Iori, 2020). A reductive phase in the early diagenesis of the rib is indicated
379 by iron oxides as pyrite pseudomorphs (framboids) near the Haversian canal
380 surfaces (see Supplementary Material). Pyrite formation and precipitation

381 typically occur in reductive environments. Iron input is derived from the
382 decomposition of organic substances, and sulfide availability is controlled by
383 collagen hydrolysis and diffusion from external sources (Pfretzschner, 2001).
384 Thus, the leaching of organic components increases the porosity of the bone
385 structure, allowing recrystallization (Pfretzschner, 2001). This process ended in
386 the early diagenesis phase, leaving the fossil barely permeable and resistant to
387 diagenetic changes (Cazalbou et al., 2004). At this stage, the deposition of
388 manganese hydroxides on apatite crystals (Figure 3D) may have occurred
389 through groundwater activity (Pfretzschner, 2004; Pfretzschner and Tütken,
390 2011).

391 The characteristics identified in the rock matrix allowed us to reconstruct
392 the palaeodepositional environment in which the final burial of the rib occurred.
393 Framework grains of diverse sizes, degrees of roundness, and different quartz
394 populations indicate that the paleoenvironment received sedimentary intake from
395 distinct sources. This petrographic feature may be related to the development of
396 the Bauru Basin during the Upper Cretaceous, which underwent a second phase
397 of uplift in its eastern region due to alkaline intrusions from the mantle (Batezelli,
398 2017; Batezelli et al., 2005; Mattos and Batezelli, 2020). Because most of these
399 grains have more angular shapes, it is suggested that their sources were closer
400 to the deposition site.

401 We propose that the deposition of the dorsal rib was rapid in a high-
402 energy system owing to the poor selection of grains from the rock framework,
403 both internally and externally, to the fossil bone. This refers to the
404 palaeodepositional system of the Marília Formation, which is characterized as
405 alluvial and dominated by progradational braided rivers with a high sediment

406 supply driven by constant avulsions and abandonment of distributive channels
407 (Batezelli, 2017). The loose packing of Bauru Basin rocks is due to calcrete
408 formation by pedogenetic and phreatic processes under semiarid and arid
409 environmental conditions (Batezelli et al., 2005; da Silva et al., 2019; Fernandes,
410 2010). Comparing the microstructure with the facies profiles from the Campina
411 Verde site (Batezelli et al., 2019), we inferred that the rib (CP2/200A-B) was
412 deposited in an ephemeral or intermittent channel bed with high sediment input
413 and was later abandoned, providing the initial fast cementation of the stratum by
414 phreatic processes over a long period of stability. During late diagenesis, an
415 oxidation stage was noted that was associated with the deposition of opaque
416 minerals on the outer surface of the bone, which were probably formed by the
417 action of rainwater (Batezelli et al., 2005). The inferred taphonomic sequence for
418 specimen CP2/200A-B is summarized in Figure 6.

419 Our findings support the hypothesis that the rapid recrystallization of
420 apatite during early diagenesis allows the preservation of bone structure, as
421 suggested by other studies on fossil bones from the Bauru Group (Marchetti et
422 al., 2019; Pinto et al., 2020). However, differences were observed in the
423 petrographic patterns proposed by Garcia et al. (2005). The presence of
424 crystalline calcite fringes on the bone surface is a feature observed in fossils from
425 the Adamantina and Uberaba Formations and is also present in this specimen
426 from the Marília Formation. To verify the proposed patterns, we recommend
427 conducting additional petrographic comparisons between specimens from the
428 Bauru Group formations.

429

430 4.3. Regional and interregional contexts

431 Specimen CP2/200A-B provides an example of bone preservation
432 associated with calcrete pedogenesis in a semi-arid climate (Batezelli et al., 2019;
433 da Silva et al., 2019). It can be used for comparison with other fossil bones found
434 in similar depositional environments around the world. Evidence of bone
435 weathering by surface exposure is present in sauropod fossils from the
436 Hasandong Formation (Paik et al., 2001), Lower Cretaceous of the Korean
437 Peninsula, and in sauropod and theropod fossils from the Neuquén Basin
438 (Previtera, 2019, 2017), Upper Cretaceous of Argentinian Patagonia. These
439 lithostratigraphic units probably indicate arid to semi-arid paleoclimates (Paik et
440 al., 2001; Previtera, 2017), further supporting the correlation between climate and
441 pre-burial weathering. In addition, pseudomorphic framboids composed of iron
442 oxides have been discovered in dinosaur bones from the Two Medicine and
443 Judith River formations of the Upper Cretaceous of North America (Rogers et al.,
444 2020), suggesting that pyrite precipitation occurred in a reducing environment
445 during initial diagenesis.

446 It is important to note that the preservation of vertebrate fossils, such as
447 bones, eggs, and coprolites, associated with pedogenesis is common in
448 Cretaceous records (e.g. Fiorillo et al., 2016; López-Martínez et al., 2000; Paik et
449 al., 2001; Therrien et al., 2009). Soils are the largest terrestrial environment, and
450 their characteristics, such as pH and redox index, are important for the
451 preservation of organic remains and the formation of fossils (Retallack, 2019).
452 For example, calcareous soils are alkaline enough to prevent the dissolution of
453 bones and shells (Retallack, 2019, 1988), favoring the preservation of the fossil
454 rib discussed in this paper. The study of paleosols that contain fossil
455 assemblages is relevant to vertebrate paleontology because it provides essential

456 information for paleoecological reconstruction and can reveal possible
457 preservation biases (Retallack, 1988; Therrien et al., 2009).

458

459

460 5. CONCLUSIONS

461 The analyses on the rib fragment (CP2/200A-B) highlighted the presence
462 of compact bone completely remodeled in the cortex and cancellous bone
463 occupying the entire medullary region.

464 Regarding taxonomic classification, the morphology of the fossil rib and
465 similarities in size suggest its classification as an indeterminate saurischian
466 dinosaur.

467 The taphonomic processes associated with the fossil rib can be
468 summarized as follows: (i) a long period of subaerial exposure of the bone,
469 followed by high-energy transport; (ii) deposition of the specimen in a reductive
470 environment with alkaline stability, recrystallization of apatite, and rapid
471 precipitation of calcite in early diagenesis, reducing fossil porosity; and (iii)
472 manganese hydroxides deposited on the apatite crystals by groundwater.

473 Finally, the study concluded that the CP2/200A-B specimen presented a
474 taphonomic bias identified among vertebrate fossils of the Bauru Group, which
475 has been reported in previous studies. Isolated fragments and the loss of bone
476 structure, even at the histological level, are recurrent signs in dinosaur
477 specimens. These characteristics may be associated with the extensive exposure
478 of bones to arid and semiarid climates, their transport into depositional
479 environments and diagenesis associated with the development of soils.

480

481

482 **Acknowledgments**

483

484 The authors thank the São Paulo Research Foundation (Fundação de
485 Amparo à Pesquisa do Estado de São Paulo, FAPESP) for the support and
486 funding of the FAPESP Project 2015/17632-5 and FAPESP Project 2019/16727-
487 3. We also thank the National Council for Scientific and Technological
488 Development (Conselho Nacional de Desenvolvimento Científico e Tecnológico
489 - CNPq) for A.B. and F.R.B. productivity grants (processes 310734/2020-7 and
490 307333/2021-3). We would like to thank Mattia Baiano for providing the
491 microscopic images of the thin sections of *Aucasaurus garridoi* ribs used for
492 comparison with the material in this study, as well as Erica Tonetto for performing
493 the electron microscopy analyses. The authors would like to thank Maria Rose
494 Petrizzo, Editor-in-Chief, and Eduardo Koutsoukos, from the advisory board of
495 the Cretaceous Research journal, reviewers Arthur S. Brum and Carlos Roberto
496 A. Candeiro, and an anonymous reviewer for their valuable suggestions, which
497 significantly improved the paper. We would like to thank Editage
498 (www.editage.com) for English language editing.

499

500

501 **REFERENCES**

502

503 Aranciaga Rolando, A.M., Motta, M.J., Agnolín, F.L., Manabe, M., Tsuihiji, T.,
504 Novas, F.E., 2022. A large Megaraptoridae (Theropoda: Coelurosauria) from

- 505 Upper Cretaceous (Maastrichtian) of Patagonia, Argentina. *Sci Rep* 12,
506 6318. <https://doi.org/10.1038/s41598-022-09272-z>
- 507 Aranciaga Rolando, M., Cerroni, M.A., Garcia Marsà, J.A., Agnolín, F. I., Motta,
508 M.J., Rozadilla, S., Brisson Eglí, F., Novas, F.E., 2021. A new medium-sized
509 abelisaurid (Theropoda, Dinosauria) from the late cretaceous (Maastrichtian)
510 Allen Formation of Northern Patagonia, Argentina. *J South Am Earth Sci* 105,
511 102915. <https://doi.org/10.1016/j.jsames.2020.102915>
- 512 Araújo Júnior, H.I. de, Marinho, T. da S., 2013. Taphonomy of a *Baurusuchus*
513 (Crocodyliformes, Baurusuchidae) from the Adamantina Formation (Upper
514 Cretaceous, Bauru Basin), Brazil: Implications for preservational modes,
515 time resolution and paleoecology. *J South Am Earth Sci* 47, 90–99.
516 <https://doi.org/10.1016/j.jsames.2013.07.006>
- 517 Aureliano, T., Ghilardi, A.M., Navarro, B.A., Fernandes, M.A., Ricardi-Branco, F.,
518 Wedel, M.J., 2021a. Exquisite air sac histological traces in a
519 hyperpneumatized nanoid sauropod dinosaur from South America. *Sci Rep*
520 11, 24207. <https://doi.org/10.1038/s41598-021-03689-8>
- 521 Aureliano, T., Ghilardi, A.M., Silva-Junior, J.C.G., Martinelli, A.G., Ribeiro, L.C.B.,
522 Marinho, T., Fernandes, M.A., Ricardi-Branco, F., Sander, P.M., 2020.
523 Influence of taphonomy on histological evidence for vertebral pneumaticity
524 in an Upper Cretaceous titanosaur from South America. *Cretac Res* 108,
525 104337. <https://doi.org/10.1016/j.cretres.2019.104337>
- 526 Aureliano, T., Nascimento, C.S.I., Fernandes, M.A., Ricardi-Branco, F., Ghilardi,
527 A.M., 2021b. Blood parasites and acute osteomyelitis in a non-avian
528 dinosaur (Sauropoda, Titanosauria) from the Upper Cretaceous Adamantina

- 529 Formation, Bauru Basin, Southeast Brazil. *Cretac Res* 118.
530 <https://doi.org/10.1016/j.cretres.2020.104672>
- 531 Azevedo, K.L., Silveira Vega, C., Fernandes, A., 2013. Taphonomic aspects of
532 vertebrate fossils from Bauru Group, Upper Cretaceous, Brazil. *Boletim*
533 *Paranaense de Geociências* 68–69, 43–51.
- 534 Baiano, M.A., Cerda, I.A., 2023. Osteohistology of *Aucasaurus garridoi*
535 (Dinosauria, Theropoda, Abelisauridae): inferences on lifestyle and growth
536 strategy. *Hist Biol* 35, 693–704.
537 <https://doi.org/10.1080/08912963.2022.2063052>
- 538 Bailleul, A.M., O'Connor, J., Schweitzer, M.H., 2019. Dinosaur paleohistology:
539 Review, trends and new avenues of investigation. *PeerJ* 2019.
540 <https://doi.org/10.7717/peerj.7764>
- 541 Bandeira, K.L.N., Brum, A.S., Pêgas, R. V., Cidade, G.M., Holgado, B., Cidade,
542 A., de Souza, R.G., 2018. The Baurusuchidae vs Theropoda record in the
543 Bauru Group (Upper Cretaceous, Brazil): a taphonomic perspective. *Journal*
544 *of Iberian Geology* 44, 25–54. <https://doi.org/10.1007/s41513-018-0048-4>
- 545 Bandeira, K.L.N., Simbras, F.M., Machado, E.B., De Almeida Campos, D.,
546 Oliveira, G.R., Kellner, A.W.A., 2016. A new giant Titanosauria (Dinosauria:
547 Sauropoda) from the Late Cretaceous Bauru Group, Brazil. *PLoS One* 11.
548 <https://doi.org/10.1371/journal.pone.0163373>
- 549 Barbosa, F.H. de S., Pereira, P.V.L.G. da C., Bergqvist, L.P., Rothschild, B.M.,
550 2016. Multiple neoplasms in a single sauropod dinosaur from the Upper
551 Cretaceous of Brazil. *Cretac Res* 62, 13–17.
552 <https://doi.org/10.1016/j.cretres.2016.01.010>

- 553 Batezelli, A., 2017. Continental systems tracts of the Brazilian Cretaceous Bauru
554 Basin and their relationship with the tectonic and climatic evolution of South
555 America. *Basin Research* 29, 1–25. <https://doi.org/10.1111/bre.12128>
- 556 Batezelli, A., Gomes, N.S., Perinotto, J.A. de J., 2005. Petrografia e evolução
557 diagenética dos arenitos da porção norte e nordeste da Bacia Bauru
558 (Cretáceo Superior). *Revista Brasileira de Geociências* 35, 311–322.
- 559 Batezelli, A., Ladeira, F.S.B., 2016. Stratigraphic framework and evolution of the
560 Cretaceous continental sequences of the Bauru, Sanfranciscana, and
561 Parecis basins, Brazil. *J South Am Earth Sci* 65, 1–24.
562 <https://doi.org/10.1016/j.jsames.2015.11.005>
- 563 Batezelli, A., Ladeira, F.S.B., Nascimento, D.L. do, da Silva, M.L., 2019. Facies
564 and palaeosol analysis in a progradational distributive fluvial system from the
565 Campanian–Maastrichtian Bauru Group, Brazil. *Sedimentology* 66, 699–
566 735. <https://doi.org/10.1111/sed.12507>
- 567 Behrensmeyer, A.K., 1978. Taphonomic and ecologic information from bone
568 weathering. *Paleobiology* 4, 150–162.
569 <https://doi.org/10.1017/S0094837300005820>
- 570 Bertini, R.J., Santucci, R.M., Arruda-Campos, A.C., 2001. TITANOSSAUROS
571 (SAUROPODA: SAURISCHIA) NO CRETÁCEO SUPERIOR
572 CONTINENTAL (FORMAÇÃO MARÍLIA, MEMBRO ECHAPORÃ) DE
573 MONTE ALTO, ESTADO DE SÃO PAULO, E CORRELAÇÃO COM
574 FORMAS ASSOCIADAS DO TRIÂNGULO MINEIRO. *Geociências* 20, 93–
575 103.
- 576 Bertini, R.J., Santucci, R.M., Toledo, C.E.V., Menegazzo, M.C., 2006.
577 TAPHONOMY AND DEPOSITIONAL HISTORY OF AN UPPER

- 578 CRETACEOUS TURTLE-BEARING OUTCROP FROM THE ADAMANTINA
579 FORMATION, SOUTHWESTERN SÃO PAULO STATE. *Rev. bras.*
580 *paleontol* 9, 181–186.
- 581 Brum, A.S., Bandeira, K.L.N., Holgado, B., Souza, L.G., Pêgas, R. V., Sayão,
582 J.M., Campos, D.A., Kellner, A.W.A., 2021a. Palaeohistology and
583 palaeopathology of an Aeolosaurini (Sauropoda: Titanosauria) from Morro
584 do Cambambe (Upper Cretaceous, Brazil). *Spanish Journal of*
585 *Palaeontology* 36, 1–18. <https://doi.org/10.7203/sjp.36.1.20305>
- 586 Brum, A.S., Bandeira, K.L.N., Sayão, J.M., Campos, D.A., Kellner, A.W.A., 2022.
587 Microstructure of axial bones of lithostrotian titanosaurs (Neosauropoda:
588 Sauropodomorpha) shows extended fast-growing phase. *Cretac Res* 136,
589 105220. <https://doi.org/10.1016/j.cretres.2022.105220>
- 590 Brum, A.S., Pêgas, R. V., Bandeira, K.L.N., Souza, L.G., Campos, D.A., Kellner,
591 A.W.A., 2021b. A new unenlagiine (Theropoda, Dromaeosauridae) from the
592 Upper Cretaceous of Brazil. *Pap Palaeontol* 7, 2075–2099.
593 <https://doi.org/10.1002/spp2.1375>
- 594 Brusatte, S.L., Candeiro, C.R.A., Simbras, F.M., 2017. The last dinosaurs of
595 Brazil: The Bauru Group and its implications for the end-Cretaceous mass
596 extinction. *An Acad Bras Cienc* 89, 1465–1485.
597 <https://doi.org/10.1590/0001-3765201720160918>
- 598 Candeiro, C.R.A., Currie, P.J., Candeiro, C.L., Bergqvist, L.P., 2017. Tooth wear
599 and microwear of theropods from the Late Maastrichtian Marília Formation
600 (Bauru Group), Minas Gerais State, Brazil, in: *Earth and Environmental*
601 *Science Transactions of the Royal Society of Edinburgh*. Cambridge

- 602 University Press, pp. 229–233.
603 <https://doi.org/10.1017/S175569101600013X>
- 604 Candeiro, C.R.D.A., Alves, D.S. de J., Gil, L.M., Figueirôa, S.F. de M., 2019. First
605 record of sauropod remains from the Maastrichtian Marília Formation (Bauru
606 group) of Monte Alegre de Minas since Friderich von Huene's description in
607 1931. *Anuario do Instituto de Geociencias* 42, 32–39.
608 https://doi.org/10.11137/2019_2_32_39
- 609 Candeiro, C.R.D.A., Brusatte, S.L., Souza, G.K. de Q., de Carvalho, A.A., Maia,
610 D.S., Dias, T.D.C., Vidal, L. da S., Gomes, M.M.N., Barros, L.M., 2020. Late
611 Cretaceous Bauru Group biota from Southern Goiás State, Brazil: History
612 and fossil content. *Earth Sciences Research Journal* 24, 387–396.
613 <https://doi.org/10.15446/esrj.v24n4.82831>
- 614 Carvalho, I. de S., Vasconcellos, F.M. de, Tavares, S.A.S., 2007.
615 *Montealtosuchus arrudacamposi*, a new peirosaurid crocodile
616 (Mesoeucrocodylia) from the Late Cretaceous Adamantina Formation of
617 Brazil. *Zootaxa* 1607, 35–46.
- 618 Castro, M.C., Goin, F.J., Ortiz-Jaureguizar, E., Vieytes, E.C., Tsukui, K.,
619 Ramezani, J., Batezelli, A., Marsola, J.C.A., Langer, M.C., 2018. A Late
620 Cretaceous mammal from Brazil and the first radioisotopic age for the Bauru
621 Group. *R Soc Open Sci* 5, 180482. <https://doi.org/10.1098/rsos.180482>
- 622 Cavalcanti, R., Candeiro, C.R. dos A., Brusatte, S.L., De Oliveira, E.F., Da Silva
623 Vidal, L., Nogueira Gomes, M.M., 2021. First dinosaur record from the
624 Marília Formation (Maastrichtian) in the Gurinhatã municipality, Minas
625 Gerais state, Brazil. *Pap Avulsos Zool* 61. [https://doi.org/10.11606/1807-](https://doi.org/10.11606/1807-0205/2021.61.75)
626 [0205/2021.61.75](https://doi.org/10.11606/1807-0205/2021.61.75)

- 627 Cazalbou, S., Eichert, D., Drouet, C., Combes, C., Rey, C., 2004. Minéralisations
628 biologiques à base de phosphate de calcium. C R Palevol 3, 563–572.
629 <https://doi.org/10.1016/j.crpv.2004.07.003>
- 630 Chinsamy, A., 2023. Palaeoecological deductions from osteohistology. Biol Lett
631 19. <https://doi.org/10.1098/rsbl.2023.0245>
- 632 Chinsamy, A., Raath, M.A., 1992. PREPARATION OF FOSSIL BONE FOR
633 HISTOLOGICAL EXAMINATION. Palaeontologia africana 29, 39–44.
- 634 Clarke, J.B., 2004. A mineralogical method to determine cyclicity in the
635 taphonomic and diagenetic history of fossilized bones. Lethaia 37, 281–284.
636 <https://doi.org/10.1080/00241160410006564>
- 637 Coria, R.A., Chiappe, L.M., Dingus, L., 2002. A new close relative of Carnotaurus
638 sastrei Bonaparte 1985 (Theropoda: Abelisauridae) from the Late
639 Cretaceous of Patagonia. J Vertebr Paleontol 22, 460–465.
640 [https://doi.org/10.1671/0272-4634\(2002\)022\[0460:ANCROC\]2.0.CO;2](https://doi.org/10.1671/0272-4634(2002)022[0460:ANCROC]2.0.CO;2)
- 641 Coria, R.A., Filippi, L.S., Chiappe, L.M., García, R., Arcucci, A.B., 2013.
642 *Overosaurus paradasorum* gen. et sp. nov., a new sauropod dinosaur
643 (Titanosauria: Lithostrotia) from the Late Cretaceous of Neuquén, Patagonia,
644 Argentina. Zootaxa 3683, 357. <https://doi.org/10.11646/zootaxa.3683.4.2>
- 645 da Silva, M.L., Batezelli, A., Ladeira, F.S.B., 2019. Genesis and evolution of
646 paleosols of the Marília Formation, Maastrichtian of the Bauru Basin, Brazil.
647 Catena (Amst) 182, 104108. <https://doi.org/10.1016/j.catena.2019.104108>
- 648 de Buffrénil, V., Quilhac, A., 2021. Bone Tissue Types: A Brief Account of
649 Currently Used Categories, in: de Buffrénil, V., de Ricqlès, A.J., Zylberberg,
650 L., Padian, K. (Eds.), Vertebrate Skeletal Histology and Paleohistology. CRC
651 Press, Boca Rato and London, pp. 147–182.

- 652 Delcourt, R., Brilhante, N.S., Grillo, O.N., Ghilardi, A.M., Augusta, B.G., Ricardi-
653 Branco, F., 2020. Carcharodontosauridae theropod tooth crowns from the
654 Upper Cretaceous (Bauru Basin) of Brazil: A reassessment of isolated
655 elements and its implications to palaeobiogeography of the group.
656 *Palaeogeogr Palaeoclimatol Palaeoecol* 556.
657 <https://doi.org/10.1016/j.palaeo.2020.109870>
- 658 Delcourt, R., Iori, F.V., 2020. A new Abelisauridae (Dinosauria: Theropoda) from
659 São José do Rio Preto Formation, Upper Cretaceous of Brazil and comments
660 on the Bauru Group fauna. *Hist Biol* 32, 917–924.
661 <https://doi.org/10.1080/08912963.2018.1546700>
- 662 Delcourt, R., Langer, M.C., 2022. A small abelisaurid caudal vertebra from the
663 Bauru Basin, Presidente Prudente Formation (Late Cretaceous), Brazil adds
664 information about the diversity and distribution of theropods in central South
665 America. *J South Am Earth Sci* 116.
666 <https://doi.org/10.1016/j.jsames.2022.103879>
- 667 Depéret, C., 1896. Note sur les Dinosauriens Sauropodes et Théropodes du
668 Crétacé supérieur de Madagascar. *Bulletin de la Société Géologique de*
669 *France* 21, 176–194.
- 670 Faria, C.C. de J., Riga, B.G., Candeiro, C.R. dos A., Marinho, T. da S., David,
671 L.O., Simbras, F.M., Castanho, R.B., Muniz, F.P., Pereira, P.V.L.G. da C.,
672 2015. Cretaceous sauropod diversity and taxonomic succession in South
673 America. *J South Am Earth Sci* 61, 154–163.
674 <https://doi.org/10.1016/j.jsames.2014.11.008>

- 675 Fernandes, L.A., 2010. Calcretes e registros de paleossolos em depósitos
676 continentais neocretáceos (Bacia Bauru, Formação Marília). Revista
677 Brasileira de Geociências 40, 19–35.
- 678 Fernandes, L.A., Coimbra, A.M., 2000. REVISÃO ESTRATIGRÁFICA DA
679 PARTE ORIENTAL DA BACIA BAURU (NEOCRETACEO). Revista
680 Brasileira de Geociências 30, 717–728.
- 681 Filippi, L.S., Méndez, A.H., Gianechini, F.A., Juárez Valieri, R.D., Garrido, A.C.,
682 2018. Osteology of *Viavenator exxoni* (Abelisauridae; Furileosauria) from the
683 Bajo de la Carpa Formation, NW Patagonia, Argentina. Cretac Res 83, 95–
684 119. <https://doi.org/10.1016/j.cretres.2017.07.019>
- 685 Fiorillo, A.R., McCarthy, P.J., Flaig, P.P., 2016. A multi-disciplinary perspective
686 on habitat preferences among dinosaurs in a Cretaceous Arctic greenhouse
687 world, North Slope, Alaska (Prince Creek Formation: lower Maastrichtian).
688 Palaeogeogr Palaeoclimatol Palaeoecol 441, 377–389.
689 <https://doi.org/10.1016/j.palaeo.2015.07.024>
- 690 Gallina, P.A., 2012. Histología Ósea del Titanosaurio Bonitasaura salgadoi
691 (Dinosauria: Sauropoda) del Cretácico Superior de Patagonia. Ameghiniana
692 49, 289–302. [https://doi.org/10.5710/AMGH.v49i3\(519\)](https://doi.org/10.5710/AMGH.v49i3(519))
- 693 Garcia, A.J.V., da Rosa, Á.A.S., Goldberg, K., 2005. Paleoenvironmental and
694 paleoclimatic control on early diagenetic processes and fossil record in
695 Cretaceous continental sandstones of Brazil. J South Am Earth Sci 19, 243–
696 258. <https://doi.org/10.1016/j.jsames.2005.01.008>
- 697 Garrido, A.C., 2010. Estratigrafía del Grupo Neuquén, Cretácico Superior de la
698 Cuenca Neuquina (Argentina): nueva propuesta de ordenamiento
699 litoestratigráfico. Rev. Mus. Argentino Cienc. Nat., n.s 12, 121–177.

- 700 Geroto, C.F.C., Bertini, R.J., 2014. Novos registros de vertebrados fósseis do
701 cretáceo superior na formação adamantina (grupo Bauru), sudeste do Brasil.
702 Revista do Instituto Geológico 35, 39–56. [https://doi.org/10.5935/0100-](https://doi.org/10.5935/0100-929x.20140008)
703 [929x.20140008](https://doi.org/10.5935/0100-929x.20140008)
- 704 Ghilardi, A.M., Aureliano, T., Duque, R.R.C., Fernandes, M.A., Barreto, A.M.F.,
705 Chinsamy, A., 2016. A new titanosaur from the Lower Cretaceous of Brazil.
706 Cretac Res 67, 16–24. <https://doi.org/10.1016/j.cretres.2016.07.001>
- 707 Iori, F.V., Araújo-Júnior, H.I. de, Tavares, S.A.S., Marinho, T. da S., Martinelli,
708 A.G., 2021. New theropod dinosaur from the Late Cretaceous of Brazil
709 improves abelisaurid diversity. J South Am Earth Sci 112.
710 <https://doi.org/10.1016/j.jsames.2021.103551>
- 711 Kremer, B., Owocki, K., Królikowska, A., Wrzosek, B., Kazmierczak, J., 2012.
712 Mineral microbial structures in a bone of the Late Cretaceous dinosaur
713 *Saurolophus angustirostris* from the Gobi Desert, Mongolia - a Raman
714 spectroscopy study. Palaeogeogr Palaeoclimatol Palaeoecol 358–360, 51–
715 61. <https://doi.org/10.1016/j.palaeo.2012.07.020>
- 716 Lamanna, M.C., Casal, G.A., Martínez, R.D.F., Ibiricu, L.M., 2020. Megaraptorid
717 (Theropoda: Tetanurae) Partial Skeletons from the Upper Cretaceous Bajo
718 Barreal Formation of Central Patagonia, Argentina: Implications for the
719 Evolution of Large Body Size in Gondwanan Megaraptorans. Annals of
720 Carnegie Museum 86. <https://doi.org/10.2992/007.086.0302>
- 721 Lamm, E.-T., 2013. Preparation and Sectioning of Specimens, in: Padian, K.,
722 Lamm, E.-T. (Eds.), Bone Histology of Fossil Tetrapods. University of
723 California Press, Berkeley and Los Angeles, California, pp. 55–160.

- 724 Lamm, E.-T., 2007. Paleohistology Widens the Field of View in Paleontology.
725 Microscopy and Microanalysis 13.
726 <https://doi.org/10.1017/s1431927607075368>
- 727 Langer, M.C., Delcourt, R., Montefeltro, F.C., Silva Junior, J.C.G., Soler, M.G.,
728 Ferreira, G.S., Ruiz, J. V., Barcelos, L.A., Onary, S., Marsola, J.C.A., Castro,
729 M.C., Cidade, G.M., Batezelli, A., 2022. THE BAURU BASIN IN SÃO PAULO
730 AND ITS TETRAPODS. Derbyana 43.
731 <https://doi.org/10.14295/derb.v43.776>
- 732 López-Martínez, N., Moratalla, J.J., Sanz, J.L., 2000. Dinosaurs nesting on tidal
733 flats. Palaeogeogr Palaeoclimatol Palaeoecol 160, 153–163.
734 [https://doi.org/10.1016/S0031-0182\(00\)00063-8](https://doi.org/10.1016/S0031-0182(00)00063-8)
- 735 Marchetti, I., 2017. HISTOLOGIA E FOSSILDIAGÊNESE DE FÓSSEIS DA
736 FORMAÇÃO ADAMANTINA, BACIA BAURU, SP. Universidade Estadual de
737 Campinas, Campinas.
- 738 Marchetti, I., Ricardi-Branco, F., Callefo, F., Delcourt, R., Galante, D., Jurigan, I.,
739 Carvalho, I.S., Tavares, S.A.S., 2019. Fossildiagenesis and ontogenetic
740 insights of crocodyliform bones from the Adamantina Formation, Bauru
741 Basin, Brazil. J South Am Earth Sci 96.
742 <https://doi.org/10.1016/j.jsames.2019.102327>
- 743 Martinelli, A.G., Teixeira, V.P.A., 2015. The Late Cretaceous vertebrate record
744 from the Bauru Group in the Triângulo Mineiro, southeastern Brazil.
- 745 Mattos, N.H.S., Batezelli, A., 2020. SOURCE - AREA, PALEOWEATHERING
746 AND PROVENANCE OF THE LATE CRETACEOUS SEQUENCES OF THE
747 BAURU BASIN (SE BRAZIL). Geosciences = Geociências 38, 943–960.
748 <https://doi.org/10.5016/geociencias.v38i4.10565>

- 749 Méndez, A.H., Gianechini, F.A., Paulina-Carabajal, A., Filippi, L.S., Juárez-
750 Valieri, R.D., Cerda, I.A., Garrido, A.C., 2022. New furileusaurian remains
751 from La Invernada (northern Patagonia, Argentina): A site of unusual
752 abelisaurids abundance. *Cretac Res* 129, 104989.
753 <https://doi.org/10.1016/j.cretres.2021.104989>
- 754 Menegazzo, M.C., Catuneanu, O., Chang, H.K., 2016. The South American
755 retroarc foreland system: The development of the Bauru Basin in the back-
756 bulge province. *Mar Pet Geol* 73, 131–156.
757 <https://doi.org/10.1016/j.marpetgeo.2016.02.027>
- 758 Mitchell, J., Sander, P.M., 2014. The three-front model: a developmental
759 explanation of long bone diaphyseal histology of Sauropoda. *Biological*
760 *Journal of the Linnean Society* 765–781.
- 761 Navarro, B.A., Ghilardi, A.M., Aureliano, T., Díaz, V.D., Bandeira, K.L.N.,
762 Cattaruzzi, A.G.S., Iori, F. V., Martine, A.M., Carvalho, A.B., Anelli, L.E.,
763 Fernandes, M.A., Zaher, H., 2022. A New Nanoid Titanosaur (Dinosauria:
764 Sauropoda) from the Upper Cretaceous of Brazil. *Ameghiniana* 59, 317–354.
765 <https://doi.org/10.5710/AMGH.25.08.2022.3477>
- 766 O'Connor, P.M., 2007. The postcranial axial skeleton of *Majungasaurus*
767 *crenatissimus* (Theropoda: Abelisauridae) from the Late Cretaceous of
768 Madagascar. *J Vertebr Paleontol* 27, 127–163. [https://doi.org/10.1671/0272-
769 4634\(2007\)27\[127:TPASOM\]2.0.CO;2](https://doi.org/10.1671/0272-4634(2007)27[127:TPASOM]2.0.CO;2)
- 770 Owocki, K., Kremer, B., Wrzosek, B., Królikowska, A., Kaźmierczak, J., 2016.
771 Fungal Ferromanganese Mineralisation in Cretaceous Dinosaur Bones from
772 the Gobi Desert, Mongolia. *PLoS One* 11.
773 <https://doi.org/10.1371/journal.pone.0146293>

- 774 Padian, K., 2013. Why Study the Bone Microstructure of Fossil Tetrapods?, in:
775 Padian, K., Lamm, E.-T. (Eds.), *Bone Histology of Fossil Tetrapods*.
776 University of California Press, Berkley and Los Angeles, California, pp. 1–
777 11.
- 778 Paes Neto, V.D., Francischini, H., Martinelli, A.G., Marinho, T.D.S., Ribeiro,
779 L.C.B., Soares, M.B., Schultz, C.L., 2018. Bioerosion traces on titanosaurian
780 sauropod bones from the Upper Cretaceous Marília Formation of Brazil.
781 *Alcheringa* 42, 415–426. <https://doi.org/10.1080/03115518.2018.1456561>
- 782 Paik, I.S., Kim, H.J., Park, K.H., Song, Y.S., Lee, Y.I., Yeon Hwang, J., Huh, M.,
783 2001. Palaeoenvironments and taphonomic preservation of dinosaur bone-
784 bearing deposits in the Lower Cretaceous Hasandong Formation, Korea.
785 *Cretac Res* 22, 627–642. <https://doi.org/10.1006/cres.2001.0282>
- 786 Pfretzschner, H.-U., 2004. Fossilization of Haversian bone in aquatic
787 environments. *C R Palevol* 3, 605–616.
788 <https://doi.org/10.1016/j.crpv.2004.07.006>
- 789 Pfretzschner, H.-U., 2001. Pyrite in fossil bone. *Neues Jahrb Geol Palaontol Abh*
790 220, 1–23. <https://doi.org/10.1127/njgpa/220/2001/1>
- 791 Pfretzschner, H.-U., Tütken, T., 2011. Rolling bones – Taphonomy of Jurassic
792 dinosaur bones inferred from diagenetic microcracks and mineral infillings.
793 *Palaeogeogr Palaeoclimatol Palaeoecol* 310, 117–123.
794 <https://doi.org/10.1016/j.palaeo.2011.01.026>
- 795 Pinto, C.B., Lacerda, M.B. da S., Rodrigues, B.L., Mussel, W. da N., Romano,
796 P.S.R., 2020. Geochemical characterization of fossil turtles from
797 Tartaruguito outcrop (Upper Cretaceous, Bauru Basin, Presidente Prudente

- 798 Formation), São Paulo state, southeastern Brazil. *J South Am Earth Sci* 104,
799 102843. <https://doi.org/10.1016/j.jsames.2020.102843>
- 800 Porfiri, J.D., Novas, F.E., Calvo, J.O., Agnolín, F.L., Ezcurra, M.D., Cerda, I.A.,
801 2014. Juvenile specimen of *Megaraptor* (Dinosauria, Theropoda) sheds light
802 about tyrannosauroid radiation. *Cretac Res* 51, 35–55.
803 <https://doi.org/10.1016/j.cretres.2014.04.007>
- 804 Previtera, E., 2019. Diagenetic Characterization of Dinosaur Remains Through
805 Histology in Fluvial Contexts from the Upper Cretaceous of the Loncoche
806 Formation, Mendoza, Argentina. *Ameghiniana* 56, 135.
807 <https://doi.org/10.5710/AMGH.16.01.2019.3235>
- 808 Previtera, E., 2017. Bone microstructure and diagenesis of saurischian dinosaurs
809 from the Upper Cretaceous (Neuquén Group), Argentina. *Andean Geology*
810 44, 39–58. <https://doi.org/10.5027/andgeoV44n1-a03>
- 811 Reis, L.F.S., Ghilardi, A.M., Fernandes, M.A., 2023. Bite traces in a sauropod rib
812 from the Upper Cretaceous São José do Rio Preto Formation (Bauru Basin),
813 Brazil. *Hist Biol* 35, 1329–1340.
814 <https://doi.org/10.1080/08912963.2022.2090248>
- 815 Retallack, G.J., 2019. *Soils of the Past: An Introduction to Paleopedology*, Third
816 Edition. ed. Wiley-Blackwell.
- 817 Retallack, G.J., 1988. Down-to-Earth Approaches to Vertebrate Paleontology.
818 *Palaios* 3, 335. <https://doi.org/10.2307/3514662>
- 819 Rogers, R.R., Regan, A.K., Weaver, L.N., Thole, J.T., Fricke, H.C., 2020.
820 Tracking authigenic mineral cements in fossil bones from the Upper
821 Cretaceous (Campanian) Two Medicine and Judith River formations,
822 Montana. *Palaios* 35, 135–150. <https://doi.org/10.2110/palo.2019.093>

- 823 Salgado, L., Carvalho, I. de S., 2008. *UBERABATITAN RIBEIROI*, A NEW
824 TITANOSAUR FROM THE MARÍLIA FORMATION (BAURU GROUP,
825 UPPER CRETACEOUS), MINAS GERAIS, BRAZIL. *Palaeontology* 51, 881–
826 901. <https://doi.org/10.1111/j.1475-4983.2008.00781.x>
- 827 Santucci, R.M., Arruda-Campos, A.C. de, 2011. A new sauropod (Macronaria,
828 Titanosauria) from the Adamantina Formation, Bauru Group, Upper
829 Cretaceous of Brazil and the phylogenetic relationships of Aeolosaurini.
830 *Zootaxa* 3085, 1. <https://doi.org/10.11646/zootaxa.3085.1.1>
- 831 Sayão, J.M., Saraiva, A.Á.F., Brum, A.S., Bantim, R.A.M., de Andrade, R.C.L.P.,
832 Cheng, X., de Lima, F.J., de Paula Silva, H., Kellner, A.W.A., 2020. The first
833 theropod dinosaur (Coelurosauria, Theropoda) from the base of the
834 Romualdo Formation (Albian), Araripe Basin, Northeast Brazil. *Sci Rep* 10.
835 <https://doi.org/10.1038/s41598-020-67822-9>
- 836 Silva Junior, J.C.G., Marinho, T.S., Martinelli, A.G., Langer, M.C., 2019.
837 Osteology and systematics of *Uberabatitan ribeiroi* (Dinosauria; Sauropoda):
838 a Late Cretaceous titanosaur from Minas Gerais, Brazil. *Zootaxa* 4577.
839 <https://doi.org/10.11646/zootaxa.4577.3.1>
- 840 Silva Junior, J.C.G., Martinelli, A.G., Iori, F. V., Marinho, T.S., Hechenleitner,
841 E.M., Langer, M.C., 2022. Reassessment of *Aeolosaurus maximus*, a
842 titanosaur dinosaur from the Late Cretaceous of Southeastern Brazil. *Hist*
843 *Biol* 34, 403–411. <https://doi.org/10.1080/08912963.2021.1920016>
- 844 Silva Junior, J.C.G., Martinelli, A.G., Marinho, T.S., da Silva, J.I., Langer, M.C.,
845 2022. New specimens of *Baurutitan britoi* and a taxonomic reassessment of
846 the titanosaur dinosaur fauna (Sauropoda) from the Serra da Galga

- 847 Formation (Late Cretaceous) of Brazil. PeerJ 10.
848 <https://doi.org/10.7717/peerj.14333>
- 849 Silva Junior, J.C.G., Martinelli, A.G., Ribeiro, L.C.B., Marinho, T.S., 2017.
850 Description of a juvenile titanosaurian dinosaur from the Upper Cretaceous
851 of Brazil. Cretac Res 76, 19–27.
852 <https://doi.org/10.1016/j.cretres.2017.03.029>
- 853 Soares, M.V.T., Basilici, G., Marinho, T. da S., Martinelli, A.G., Marconato, A.,
854 Mountney, N.P., Colombera, L., Mesquita, Á.F., Vasques, J.T., Junior,
855 F.R.A., Ribeiro, L.C.B., 2021. Sedimentology of a distributive fluvial system:
856 The Serra da Galga Formation, a new lithostratigraphic unit (Upper
857 Cretaceous, Bauru Basin, Brazil). Geological Journal 56, 951–975.
858 <https://doi.org/10.1002/gj.3987>
- 859 Souza, G.A. de, Soares, M.B., Brum, A.S., Zucolotto, M., Sayão, J.M.,
860 Weinschütz, L.C., Kellner, A.W.A., 2020. Osteohistology and growth
861 dynamics of the Brazilian noosaurid *Vespersaurus paranaensis* Langer et
862 al., 2019 (Theropoda: Abelisauroidea). PeerJ 8.
863 <https://doi.org/10.7717/peerj.9771>
- 864 Tavares, S.A.S., Ricardi Branco, F., Santucci, R.M., 2014. Theropod teeth from
865 the Adamantina Formation (Bauru Group, Upper Cretaceous), Monte Alto,
866 São Paulo, Brazil. Cretac Res 50, 59–71.
867 <https://doi.org/10.1016/j.cretres.2014.03.021>
- 868 Therrien, F., Zelenitsky, D.K., Weishampel, D.B., 2009. Palaeoenvironmental
869 reconstruction of the Late Cretaceous Sânpetru Formation (Hațeg Basin,
870 Romania) using paleosols and implications for the “disappearance” of

- 871 dinosaurs. *Palaeogeogr Palaeoclimatol Palaeoecol* 272, 37–52.
872 <https://doi.org/10.1016/j.palaeo.2008.10.023>
- 873 Vasconcellos, F.M. de, Carvalho, I. de S., 2006. CONDICIONANTE
874 ETOLÓGICO NA TAFONOMIA DE *UBERABASUCHUS TERRIFICUS*
875 (CROCODYLIFORMES, PEIROSOURIDAE) DA BACIA BAURU
876 (CRETÁCEO SUPERIOR). *Geociências* 25, 225–230.
- 877 Waskow, K., Sander, P.M., 2014. GROWTH RECORD AND HISTOLOGICAL
878 VARIATION IN THE DORSAL RIBS OF *CAMARASAURUS* SP.
879 (SAUROPODA). *J Vertebr Paleontol* 34, 852–869.
- 880 Wilson, J.A., 2002. Sauropod dinosaur phylogeny: critique and cladistic analysis.
881 *Zool J Linn Soc* 136, 215–275. [https://doi.org/10.1046/j.1096-](https://doi.org/10.1046/j.1096-3642.2002.00029.x)
882 [3642.2002.00029.x](https://doi.org/10.1046/j.1096-3642.2002.00029.x)
- 883 Windholz, G.J., González, R., Cerda, I.A., Bellardini, F., Silva, J.C.G., Marinho,
884 T.S., Ribeiro, L.C.B., Martinelli, A.G., 2023. Osteohistology of *Uberabatitan*
885 *ribeiroi* (Dinosauria, Sauropoda) provides insight into the life history of
886 titanosaurs. *Hist Biol*. <https://doi.org/10.1080/08912963.2023.2253257>
- 887 Wings, O., 2004. Authigenic minerals in fossil bones from the Mesozoic of
888 England: poor correlation with depositional environments. *Palaeogeogr*
889 *Palaeoclimatol Palaeoecol* 204, 15–32. [https://doi.org/10.1016/S0031-](https://doi.org/10.1016/S0031-0182(03)00709-0)
890 [0182\(03\)00709-0](https://doi.org/10.1016/S0031-0182(03)00709-0)
- 891
- 892
- 893
- 894
- 895

896 **FIGURE CAPTIONS**

897

898 Figure 1. Location of the outcrop in Brazil where the fossil studied was collected.

899 A, extension of the Bauru Basin in the Brazilian territory and position of the
900 outcrop in the Triângulo Mineiro region (stratigraphy based on Batezelli, 2017).901 B, and C, sampling site and the rib fragment position in the outcrop stratigraphic
902 column (modified from on Batezelli, 2019). B, view of outcrop next to BR 364
903 highway. B. layer in which the fossil was found (petrographic hammer for size
904 reference = 30cm).

905

906 Figure 2. Pictures of the rib fragment before (left side) and after (right side)

907 cutting. A, and B, transverse view of the rib (CP2/200A), highlighting the eroded

908 lateral region of the bone (arrow) and the rock matrix layer (arrow). C, and D,

909 longitudinal view of the rib (CP2/200B), highlighting the eroded region (arrow)

910 and a fine layer of rock (arrow) still covering to the fossil. Section CP2/200A is

911 represented on the slide 234 and CP2/200B on the slide 235. Scale bars = 20mm.

912

913 Figure 3. Petrography of the rib fragment of the sample CP2/200A (slide 234). A,

914 panoramic view of transverse section, the arrow show point to the fine layer of

915 residual rock on the side of the bone, natural light. B, secondary osteon at the

916 edge of the cortex, with extensive fracture present on the right under natural light.

917 C, Damaged second-generation osteon, arrow showing overlap, polarized light

918 with gypsum compensator. D, osteon in natural light with the presence of

919 dendrites in its lamellae, indicates by arrow. E, bone remodeling region with a

920 large erosion cavity (white arrow), vein (black arrow) and replacement process of

921 bone tissue by calcite, natural light. Scale bar= 10mm in A; 500 μ m in B, C, E;
922 250 μ m in D. C = calcite (sparite and micrite)

923

924 Figure 4. Petrography of the rib fragment of the sample CP2/200B (slide 235). A,
925 panoramic view of transverse section, the arrow show point to the fine layer of
926 residual rock on the side of the bone, natural light. B, damaged secondary osteon
927 observed under polarized light with gypsum compensator. C, medullary region,
928 with the presence of trabeculae and erosion cavities, pointed by arrows, polarized
929 light with gypsum compensator. Scale bar= 10mm in A; 500 μ m in B, C. Legend:
930 C = calcite (sparite and micrite).

931

932 Figure 5. Microscopy of observed mineral grains and diagenetic structures. A,
933 rounded polycrystalline quartz with slightly eroded edges (center), close to an
934 isolated secondary osteon (upper right), both surrounded by calcitic matrix and
935 cement, polarized light. B, quartz grain with features, indicates by arrow,
936 polarized light. C, rounded plagioclase feldspar grain (arrow), with eroded edges,
937 polarized light. D, subangular microcline feldspar grain (arrow), with eroded
938 edges, close to the bone trabeculae under the process of initial tissue
939 replacement by calcite ("shading" effect), shows by arrow, polarized light. E,
940 rounded grain of volcanic-like texture (center) with partial replacement, polarized
941 light. F, grain peloidal texture (center) with spatic calcite overlay (arrow), natural
942 light. Scale bar= 500 μ m in A, B, C, D, E, F. Legend: C = calcite (sparite and
943 micrite), T= trabeculae, Os = secondary osteon.

944

945 Figure 6. Diagram of the sequence of taphonomic processes inferred for the fossil
946 rib fragment CP2/200A-B. I, exposure of the bone on the ground surface,
947 associated with pre-burial weathering and abrasion. II, deposition of the
948 specimen in a reducing environment, inducing the precipitation of framboidal
949 pyrite on the inner spaces of the bone. III, deposition of manganese oxides on
950 apatite crystals due to groundwater action, followed by calcite cementation
951 related to pedogenesis. IV, deposition of opaque minerals on the bone's surface,
952 associated with leaching by rainwater action.

ARTICLE HIGHLIGHTS

TAPHONOMY AND PALEOHISTOLOGY OF A DINOSAUR RIB FROM MARÍLIA FORMATION, BAURU GROUP, IN THE STATE OF MINAS GERAIS, BRAZIL

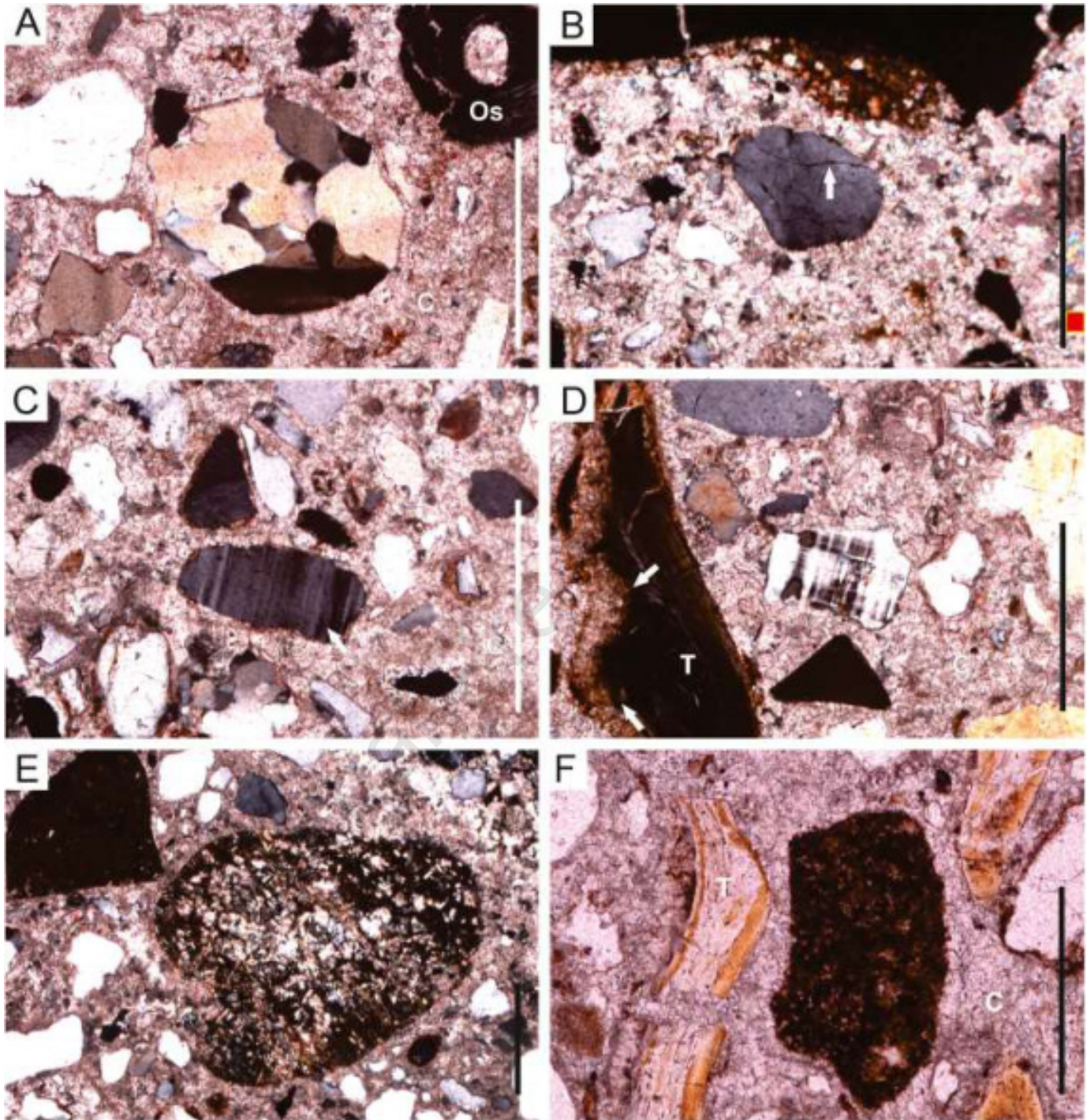
- Loss of histological structures due to transport and bone weathering
- Fossil preservation associated with bone exposure and burial on semiarid climate
- Hypothesis support a taphonomic bias in dinosaur fossils from the Bauru Group

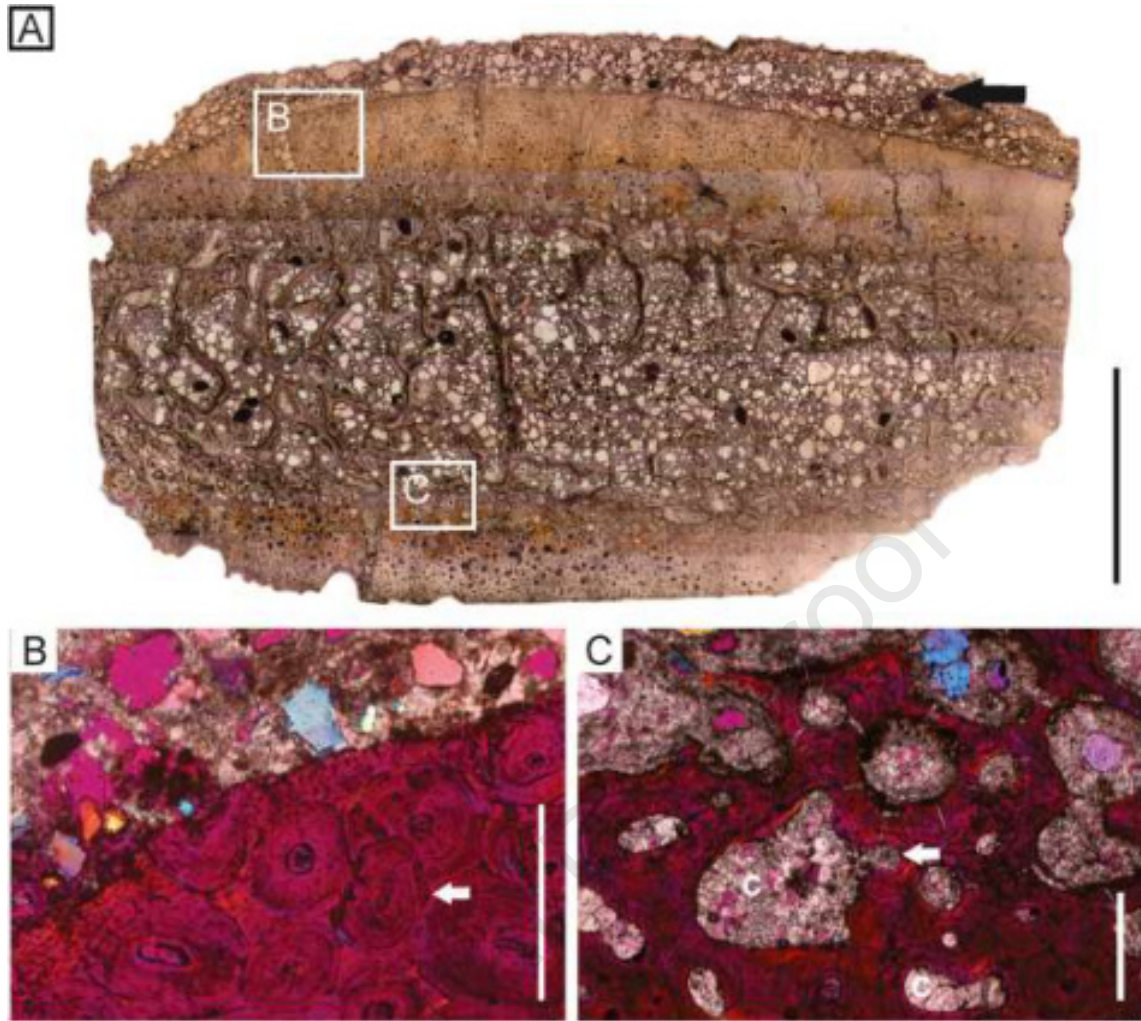
Declaration of interests

The authors declare that they have no known competing financial interests or personal relationships that could have appeared to influence the work reported in this paper.

The authors declare the following financial interests/personal relationships which may be considered as potential competing interests:

Journal Pre-proof





A

